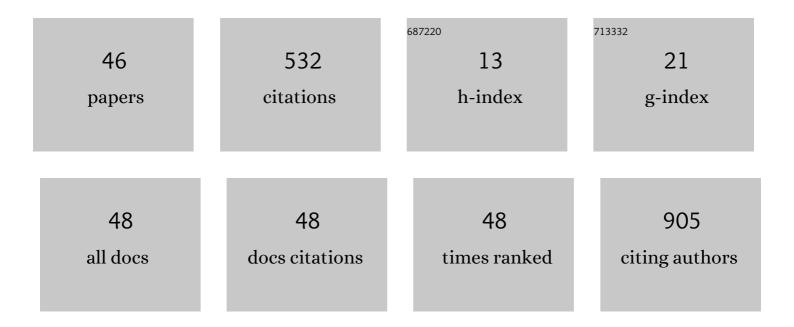
Yu Gong

List of Publications by Year in descending order

Source: https://exaly.com/author-pdf/8034628/publications.pdf

Version: 2024-02-01



#	Article	IF	CITATIONS
1	Toward a Unified Identification of Ti Location in the MFI Framework of High-Ti-Loaded TS-1: Combined EXAFS, XANES, and DFT Study. Journal of Physical Chemistry C, 2016, 120, 20114-20124.	1.5	45
2	Synthesis and structural characterization of ZnO doped with Co. Journal of Alloys and Compounds, 2013, 558, 212-221.	2.8	43
3	Pressure-induced superconductivity and structural transition in ferromagnetic <mml:math xmlns:mml="http://www.w3.org/1998/Math/MathML"><mml:msub><mml:mi mathvariant="normal">CrSiTe<mml:mn>3</mml:mn></mml:mi </mml:msub>. Physical Review B. 2020. 102</mml:math 	1.1	39
4	Crystallization mechanism analysis of noncrystalline Ni–P nanoparticles through XRD, HRTEM and XAFS. CrystEngComm, 2014, 16, 9657-9668.	1.3	33
5	Time-Resolved Small-Angle X-ray Scattering Study on the Growth Behavior of Silver Nanoparticles. Journal of Physical Chemistry C, 2014, 118, 11454-11463.	1.5	29
6	In-situ microstructural changes of polyacrylonitrile based fibers with stretching deformation. Polymer, 2014, 55, 4270-4280.	1.8	26
7	V ₂ O ₅ nanobelt arrays with controllable morphologies for enhanced performance supercapacitors. CrystEngComm, 2017, 19, 6412-6424.	1.3	23
8	Tertiary structure of cactus-like WO 3 spheres self-assembled on Cu foil for supercapacitive electrode materials. Journal of Alloys and Compounds, 2017, 712, 345-354.	2.8	21
9	Preparation and supercapacitive property of molybdenum disulfide (MoS2) nanoflake arrays- tungsten trioxide (WO3) nanorod arrays composite heterojunction: A synergistic effect of one-dimensional and two-dimensional nanomaterials. Electrochimica Acta, 2018, 263, 409-416.	2.6	21
10	Quantum phase transition from superconducting to insulating-like state in a pressurized cuprate superconductor. Nature Physics, 2022, 18, 406-410.	6.5	18
11	Nanostructural hereditability in polyacrylonitrile based fibers studied by small angle X-ray scattering. Polymer, 2018, 153, 485-497.	1.8	17
12	Microstructural change of degummed Bombyx mori silk: An in situ stretching wide-angle X-ray-scattering study. International Journal of Biological Macromolecules, 2013, 57, 99-104.	3.6	16
13	Hydrothermal preparation of MoS 2 nanoflake arrays on Cu foil with enhanced supercapacitive property. Electrochimica Acta, 2017, 227, 101-109.	2.6	15
14	Synthesis of Two-Dimensional CsPb ₂ X ₅ (X = Br and I) with a Stable Structure and Tunable Bandgap by CsPbX ₃ Phase Separation. Journal of Physical Chemistry Letters, 2022, 13, 2555-2562.	2.1	14
15	Optimal synthesis and magnetic properties of size-controlled nickel phosphide nanoparticles. Journal of Alloys and Compounds, 2014, 605, 230-236.	2.8	13
16	Magnetism variation of the compressed antiferromagnetic topological insulator EuSn2As2. Science China: Physics, Mechanics and Astronomy, 2021, 64, 1.	2.0	13
17	Mythen detector for X-ray diffraction at the Beijing synchrotron radiation facility. Instrumentation Science and Technology, 2016, 44, 1-11.	0.9	12
18	Biâ€centric view of the isostructural phase transitions in αâ€Bi ₂ Se ₃ and αâ€Bi ₂ Te ₃ . Physica Status Solidi (B): Basic Research, 2017, 254, 1700007.	0.7	11

Yu Gong

#	Article	lF	CITATIONS
19	Structural Change of Human Hair Induced by Mercury Exposure. Environmental Science & Technology, 2013, 47, 11214-11220.	4.6	10
20	Comparative investigation of the vibrational properties of bulk 2 <i>H</i> –MoS ₂ and its exfoliated nanosheets under high pressure. Journal of Raman Spectroscopy, 2017, 48, 596-600.	1.2	10
21	Revisiting local structural changes in GeO ₂ glass at high pressure. Journal of Physics Condensed Matter, 2017, 29, 465401.	0.7	8
22	Structural changes in hexagonal WO3 under high pressure. Journal of Alloys and Compounds, 2019, 797, 1013-1017.	2.8	8
23	Prediction of topological nontrivial semimetals and pressure-induced Lifshitz transition in 1T′-MoS ₂ layered bulk polytypes. Nanoscale, 2020, 12, 22710-22717.	2.8	8
24	Local structural changes during the disordered substitutional alloy transition in Bi2Te3 by high-pressure XAFS. Journal of Applied Physics, 2018, 124, 065901.	1.1	7
25	Local insight into the La-induced structural phase transition in multiferroic BiFeO ₃ ceramics by x-ray absorption fine structure spectroscopy. Journal of Physics Condensed Matter, 2019, 31, 085402.	0.7	7
26	In Situ Time-Resolved X-ray Absorption Fine Structure and Small Angle X-ray Scattering Revealed an Unexpected Phase Structure Transformation during the Growth of Nickel Phosphide Nanoparticles. Journal of Physical Chemistry C, 2018, 122, 16397-16405.	1.5	6
27	Equation of state of LiCoO ₂ under 30 GPa pressure. Chinese Physics B, 2019, 28, 016402.	0.7	6
28	Pressure-induced phase transitions, amorphization and alloying in Sb ₂ S ₃ . Physical Chemistry Chemical Physics, 2022, 24, 10053-10061.	1.3	6
29	Noncrystalline structure of Ni–P nanoparticles prepared by liquid pulse discharge. Journal of Synchrotron Radiation, 2015, 22, 376-384.	1.0	5
30	High Pressure Induced in Situ Solid-State Phase Transformation of Nonepitaxial Grown Metal@Semiconductor Nanocrystals. Journal of Physical Chemistry Letters, 2018, 9, 6544-6549.	2.1	5
31	Temperature-driven directional coalescence of silver nanoparticles. Journal of Synchrotron Radiation, 2016, 23, 718-728.	1.0	4
32	Application of Mythen detector: In-situ XRD study on the thermal expansion behavior of metal indium. Science China: Physics, Mechanics and Astronomy, 2016, 59, 1.	2.0	4
33	Pressure-induced phase transitions and structural evolution across the insulator–metal transition in bulk and nanoscale BiFeO ₃ . Journal of Physics Condensed Matter, 2019, 31, 265404.	0.7	4
34	Probing temperature effects on lattice distortion and oxidation resistance of high-entropy alloys by in situ SR-XRD and XANES. Journal of Materials Research, 2021, 36, 4413-4425.	1.2	4
35	Shape evolution with temperature of a thermotolerant protein (<i>PeaT</i> 1) in solution detected by small angle Xâ€ray scattering. Proteins: Structure, Function and Bioinformatics, 2013, 81, 53-62.	1.5	3
36	Local insight to the structural phase transition sequence of Bi ₂ Se ₃ under quasi-hydrostatic and nonhydrostatic pressure. Journal of Physics Condensed Matter, 2021, 33, 215402.	0.7	3

Yu Gong

#	Article	IF	CITATIONS
37	GISAXS and SAXS studies on the spatial structures of Co nanowire arrays. Chinese Physics C, 2011, 35, 875-879.	1.5	2
38	Anharmonicity and local lattice distortion in strained Ge-dilute Si1â^'Ge alloy. Journal of Alloys and Compounds, 2015, 653, 117-121.	2.8	2
39	LaB\${}_{6}\$ Work Function and Structural Stability under High Pressure. Chinese Physics Letters, 2017, 34, 076201.	1.3	2
40	Phase transitions in bismuth under rapid compression. Chinese Physics B, 2019, 28, 036201.	0.7	2
41	Anomalous lattice stiffening in tungsten tetraboride solid solutions with manganese under compression. Journal of Physics Condensed Matter, 2020, 32, 165702.	0.7	2
42	Redox-Induced Destabilization of Dolomite at Earth's Mantle Transition Zone. Journal of Earth Science (Wuhan, China), 2021, 32, 880-886.	1.1	2
43	Hierarchical structure and biomineralization in cricket teeth. Chinese Physics C, 2013, 37, 028001.	1.5	1
44	Anomalous enhancement of atomic vibration induced by electronic transition in 2H-MoTe2 under compression. Journal of Physics Condensed Matter, 2021, 34, .	0.7	1
45	Unusual suppression of tungsten 5d electron depletion in superhard tungsten tetraboride solid solution with chromium under compression. Journal of Physics Condensed Matter, 2022, 34, 035401.	0.7	1
46	Biâ€centric view of the isostructural phase transitions in αâ€Bi ₂ Se ₃ and αâ€Bi ₂ Te ₃ (Phys. Status Solidi B 7/2017). Physica Status Solidi (B): Basic Research, 2017, 254, 1770238.	0.7	0